NISTIR 6588

FIFTEENTH MEETING OF THE UJNR PANEL ON FIRE RESEARCH AND SAFETY MARCH 1-7, 2000

VOLUME 2

Sheilda L. Bryner, Editor

National Institute of Standards and Technology
Technology Administration, U.S. Department of Commerce

NISTIR 6588

FIFTEENTH MEETING OF THE UJNR PANEL ON FIRE RESEARCH AND SAFETY MARCH 1-7, 2000

VOLUME 2

Sheilda L. Bryner, Editor

November 2000

U. S. Department of Commerce
Norman Y. Mineta, Secretary
Technology Administration
Dr. Cheryl L. Shavers, Under Secretary of Commerce for Technology
National Institute of Standards and Technology
Raymond G. Kammer, Director

Simultaneous Measurements of Drop Size and Velocity in Large-Scale Sprinkler Flows Using Laser-Induced Fluorescence

David Everest and Arvind Atreya
Department of Mechanical Engineering and Applied Mechanics
University of Michigan, Ann Arbor, MI 48109-2125

ABSTRACT

This paper reports an experimental technique that is developed for instantaneous planar measurements of droplet size and velocity for dilute sprays in general and sprinkler sprays in particular. This particle tracking technique relies on photographic measurements of fluorescence and Mie scattering from water droplets to determine their size and velocity. Measurements were made in a plane that passes through the vertical axis of symmetry of a specially designed axis-symmetric sprinkler. Drop sizes down to $0.2mm$, within the $250\,mm \times 350\,mm$ viewing area, were measured from the digitized photographs. Drop velocities were determined from the same double-exposed photographs and the directional ambiguity was resolved by color differentiation of fluorescence vs. scattering. Dye selection and its concentration was determined by testing the fluorescence output of water tracer dyes. Collection optics and laser power was varied to optimize the color differentiation and maximize the resolution for drop size measurements.

INTRODUCTION

Water spray sprinklers are the most commonly used automatic fire protection systems in buildings ranging from small offices to large warehouses. For effective fire suppression, the sprinkler water must reach the burning surface. An optimum sprinkler system, for a given application, is one that provides the maximum fraction of water delivered by the sprinkler (or sprinklers in a large warehouse) to the burning surfaces and suppresses the fire in the shortest time after its initiation. The design of such a sprinkler system depends on the geometrical relationship between the sprinkler(s) and the fire source and its heat release rate, the geometry of the room and its ventilation conditions and the sprinkler spray characteristics. Given the complexity of the problem, the optimization, as well as the evaluation, of various sprinkler systems is most cost-effectively accomplished via computer models that can calculate the fire and sprinkler induced flows for different geometries. Such models have been developed at BFRL (NIST) by McGrattan, Baum and Rehm [see Ref. 1 & references therein]. For experimental validation of these models, instantaneous field measurements are needed on drop size distribution, drop velocity, sprinkler induced flows, and the actual delivered density. This paper develops a laser-based technique to provide the data on drop size distribution and drop velocities.

A number of standard techniques and instruments are available for measuring drop size distributions in sprays such as Phase-Doppler Anemometer (PDA) [2] and Particle Measuring System (PMS) [3]. These techniques are suitable for measuring a single point or an array of points, but do not provide the instantaneous spatial drop distribution in the spray. Consequently, a large number of measurements must be taken at different points to determine the drop-size distributions and the spray must be considered time invariant. To overcome this difficulty, an axis-symmetric sprinkler was designed and instantaneous planar measurements were made along the vertical axis of the sprinkler spray. Different techniques of simultaneous planar measurement of droplet size and velocity have recently appeared in the literature. Kadambi et al. [4] have identified the errors associated with particle size measurements from Particle Image Velocimetry (PIV) images. Herpfer and Jeng [5] have introduced streak PIV for planar measurements of droplet sizes and velocities. Cao et al. [6] have used planar laser-induced fluorescence for measurements of droplet size and Particle Tracking Velocimetry (PTV) for measuring drop velocities. The PTV technique is similar to the PIV technique and is useful when the density of seed particles is low. In this paper, we present a Particle Tracking Velocimetry and Imaging (PTVI) technique, similar to Cao et al. [6], that relies on taking instantaneous double-exposed color photographs of the spray and using them to obtain both velocities and particle sizes. Since the double-exposed photographs are created by laser shots of two different wavelengths, the color differentiation also helps resolve the flow direction.

EXPERIMENTAL TECHNIQUE

Droplet Sizing Considerations

Sizing and tracking a particle in a large field of view (FOV) requires simultaneously satisfying disparate requirements of low magnification and high spatial resolution. For proper sizing, the spatial resolution of the optical, film and digital components must result in a fully resolvable drop, indicating as large a magnification as possible. Meeting the spatial requirements for drop sizing results in limiting the FOV and a subsequent loss in the dynamic velocity resolution and the dynamic spatial resolution, as defined by Adrian [6]. Greater than optimal magnification required to meet the sizing requirements reduces the spatial and velocity spectrums over which the velocity measurements can be made.

Kadambi et al. [4] identify the effects that must be considered in properly resolving the drop size. In their experiments, scattering from solid particles suspended in a liquid was measured. They identified effects of spatial resolution, light sheet intensity distribution, and depth of field (DOF) on particle size measurements. It was observed that the particle image should be greater than 3 pixels in diameter to accurately determine its size. In quantifying the light sheet intensity distribution effect and the DOF effect, they used a 200 μm particle, a DOF of 200 μm and a beam sheet thickness of 1600 μm. By moving the focused particle through the light sheet, they observed a decrease in the measured diameter of approximately 9% and a roughly 50% decrease in scattered light intensity at the edges of the light sheet relative to the center. In another experiment, they traversed the imaging camera while holding the particle and laser sheet fixed to determine the effect of DOF. It was observed that the particle diameter increased by approximately 9%, while the intensity level again decreased by roughly 50%. Thus, when a particle is not centered in the light sheet and the focal plane, DOF and beam sheet intensity effects approximately cancel each other out resulting in a constant particle diameter. Their reported particle diameters had a standard deviation of 7%.

While Kadambi et al. [4] and Adrian's [6] results were very helpful, scattering measurements did not yield a reliable droplet size in the present work perhaps due to a greater disparity in the index of refraction between air and water. Thus, planar fluorescence imaging along with scattering was used to make drop size and velocity measurements in a large FOV with low-density sprinkler spray. The fluorescence emission signal 'F' for droplets is given by the equation:

$$F \sim \phi I_O \, \nu (m/(m+1)/f\#)^2 \, V c R \qquad (1)$$

Here, 'F' is proportional to the fluorescence yield 'ϕ', intensity of light incident on the droplet 'I_O', frequency of emitted light 'ν' and the volume of the illuminated droplet 'V'. The signal is nonlinearly related to the magnification 'm', $f\#$, the dye concentration 'c' and the film response function 'R'. The scattering signal for large water drops in a low-density spray is given by:

$$S \sim I_0 \, \nu (m/(m+1)/f\#)^2 A \, \tau R \qquad (2)$$

The signal 'S' is linearly related to 'I_0' – the incident intensity, ν – the frequency of scattered light and 'A' – the area of the illuminated drop. It is nonlinearly related to the magnification 'm', f#, the angle of incidence of a light ray on the drop 'τ', and the film response function 'R'. For both cases, the signal quality is improved by using higher magnifications and smaller $f\#s$. However, to meet the FOV requirements the magnification is fixed at 0.1, and only $f\#$ can be reduced.

The response function 'R' of the film is dependent on the spectral and exposure response characteristics of the film emulsions. Characteristic sensitivity curves for Kodak Pro film were used to define the film spectral response function. These curves indicate that the film is 30 times more sensitive for 588nm (fluorescence) and 532nm (scattering) than for 355nm UV scattered light. The increased energy in the shorter UV wavelength improves the signal but lower 355nm laser power offsets that gain. As a result, 355nm scattering was observed only in a few images.

Tests were conducted to identify the effect of fluorescent dye concentration, resolution of the imaging system, effect of variation in laser sheet intensity and effect of laser sheet power. The results of these tests are used to

quantify the ability of the measuring system to accurately characterize the spray velocities and particle size while maximizing FOV.

Experimental Setup

Fig. 1 schematically shows the experimental layout for the droplet velocity and size distribution measurements. Water exits through a 8*mm* diameter nozzle at 5 gallons/min and impinges on a conical strike plate creating the sprinkler spray. A fluorescent tracer dye is injected into the water far upstream of the nozzle. A dual-pulse ND:YAG laser provides two laser beams that are formed into light sheets by a single f6.35 mm diverging cylindrical lens. The leading beam sheet, formed by the third harmonic (355*nm*)occurs 1 millisecond prior to the lagging beam sheet, which results from the second harmonic (532*nm*) of the second ND:YAG laser. Fluorescence and Mie scattered light from the two laser pulses is captured by a 35*mm* color film camera using a 50*mm* f1.2 lens with 800 ASA Fujicolor film. Since the framing rate of the film camera is too low to obtain images on separate frames, the photographs were double exposed. Time discrimination was obtained by the fluorescent dye that created different color droplet images for the two laser pulses firing at two different wavelengths. To control the scattering signal at 532 nm, Quantaray R2 red filter or Schotts OG530 was used to allow only the fluorescence signal and some portion of the scattered signal to reach the film. Images of water droplets in a region 250*mm* x 350*mm* and 300*mm* downstream of the strike plate were taken at a magnification of 0.1 to characterize the droplet size and velocity. The negatives were digitized with a 4000*dpi* Polaroid film scanner that resulted in a digital resolution of 71 μm in the droplet plane/pixel (based on scattering from two fibers at a known distance apart). The optical spatial resolution of the imaging system was also measured by using a standard USAF resolution chart. Images were obtained at a magnification of 0.1 for various *f#s*. The best resolution obtained was for an *f#* of 2.8 at 3.17 *lp/mm* i.e. a line 158 μm thick can be resolved in the droplet plane. This corresponds to roughly 2 pixels in the image. Assuming that 3x3 pixels are needed to measure the drop size with reasonable accuracy, we obtain the minimum measurable droplet diameter of about 0.2*mm*.

The digitized images were processed using the TSI Insight and SCION Image software for determining the droplet velocities and droplet size respectively. These images had sufficient spatial resolution for sizing 0.2*mm* diameter droplets, as well as, color differentiation for resolving the directional ambiguity in velocity measurements. For a laser pulse separation of 1*ms*, velocities in the range of 0.2 *m/s* (for small drops) to 10 *m/s* (for large drops) could be measured.

Determination of Fluorescent dye Concentrations

Proper choice of the fluorescent dye and its concentration must be made to obtain the best signal. Two types of water tracing dyes with high fluorescence yield, red rhodamine and yellow/green fluoroscein, can be injected into the water stream 1.5 meters upstream of the nozzle exit (to ensure mixing) as shown in Figure 1. Different concentrations of these dyes were tested by passing a beam through a glass tube filled with the mixture. The emissions were imaged onto videotape by a Cohu CCD array camera with a f2.8 lens and Schott OG550, and analyzed using a Data Translation frame-grabber board and Image-Pro software. The relative emission curves of the rhodamine and fluoroscein dye are shown in Figure 2. Emissions from the excitation due to the UV, 355 nm, laser and the visible, 532 nm, laser are indicated. The laser power was intentionally low at 5 mJ/shot to simulate the laser fluence that exists in the sprinkler experiment.

A number of striking observations can be made from Figure 2. At low concentrations, the rhodamine dye is much better at fluorescing than the fluoroscein dye for both excitation wavelengths. The 355*nm* excitation is more effective than excitation at 532*nm* for low fluoroscein dye concentrations. The rhodamine dye reaches a maximum fluorescence signal at approximately 0.005*g/l*, and this maximum is reached earlier at 532*nm*. The fluoroscein dye reaches a maximum near a concentration of 0.05*g/l*, and again the stronger excitation wavelength, 355*nm*, reaches the maximum first. Absorption was also qualitatively measured and observations indicated that the rhodamine dye is the more effective dye for absorbing both excitation wavelengths. The 532*nm* excitation was more effectively absorbed than the 355*nm* excitation. Beyond 0.1*g/l*, both dyes have a high absorption that reduces the emissions.

In a different set of experiments, a Schotts OG530 filter replaced the OG550 filter in front of the CCD camera, allowing some 532*nm* scattering to be imaged. 532*nm* scattering from air bubbles was observed to have a signal that is equal to 75% of the net fluorescence signal at a concentration of 0.0066*g/l*. Since the scattering of a water drop in air is expected to be 10 times greater than an air bubble in water, clearly scattering will be dominant in the sprinkler flow when fluoroscein dye is used. When rhodamine dye is used, test results indicate that scattering and fluorescence will be of the same order of magnitude with the OG530 filter.

For imaging droplets, rhodamine dye was used at a concentration of 3.3*mg/l*. If used at higher concentrations, Figure 2 indicates that the signal would not increase due to absorption of the laser beam. If used at lower concentrations, the UV fluorescence signal becomes too weak. As shown below, scattering appears to dominate the drop signal except when it is fully in the laser sheet, where the scattering vs. fluorescence signal depends on the scattering angle.

Identification of Minimum Signal Levels

It is instructive to understand how the fluorescence signal varies as the drop size changes and the *f#* of the optics is varied. This was investigated by imaging fluorescence from a 2.8*mm*± 5% diameter drop that was centered in the 355*nm* laser light sheet and centered in the depth of field of the camera. A long-pass 550*nm* filter was used to collect fluorescence at 588*nm* that results from 355*nm* excitation. Images were taken at a magnification '*m*' of 0.09 for *f#s* of 1.2, 2.8, 4.0 and 5.6. The laser intensity was 2.2 times higher than that in the spray experiments. The measured droplet diameters were 2.7*mm* ± 10%.

The change in the relative maximum intensity with *f#* is shown in Fig.3 for *f#s* of 1.2, 2.8, 4.0 and 5.6. The average background signal of 34 was subtracted from the data in Figure 3. From Equ. (1) the signal is proportional to *volume/f#*^{2}. Thus, the intensity is plotted against 1/f#^{2},which should result in a linearly increasing function, but it is clearly not linear across the entire range. The two highest*f#s* (4.0 & 5.6) were used to fit a line through the origin. This line defines the expected intensity level for the 2.8*mm* drop. However, at *f#* of 1.2, the intensity is significantly lower than the expected level.

A reason for this drop in the signal level can be found in the depth of field (δz), calculated according to [6]: $\delta z = 4(1 + m^{-1})^2 f\#^2 \lambda$. For a given magnification and wavelength, the depth of field becomes 3*mm* for *f#* greater than 2.8. However for *f#* of 1.2, the depth of field is only 0.5*mm*, much smaller than the drop diameter. As discussed below, the 355 *nm* beam sheet FWHM was 3.5*mm*, much larger than the depth of field and slightly larger than the drop. The drop is therefore fully illuminated, however the fluorescence outside the depth of field is not in focus and therefore does not increase the signal as anticipated. Hence, the depth of field serves to limit the fluorescence volume used in Eq. (1) for drops that are larger than the depth of field. The fluorescence volume is proportional to $\delta z \times (drop - dia.)^2$. Since, δz is also proportional to *f#*^{2}, it would appear that for drops larger than the depth of field, the intensity should not depend on the*f#*. However, there is some increase as indicated by the dotted line in figure 3; the reason is that the portion out of the depth of field still makes some contribution to the signal.

For small drops that are less than a pixel wide, the fluorescence intensity (Equ.(1)) is proportional to the volume of the drop. For diameters greater than the pixel size, the maximum fluorescence volume is proportional to the *pixel area x drop diameter* until the depth of field limit is reached. Thus, the question arises: What is the minimum diameter at which fluorescence signal can be determined above the noise? The answer to this question can be estimated from Figure 3 if the background noise level is known. From the drop images it was determined that noise in the background signal level is 10% of 34, indicating that intensity levels below 7 will have a signal to noise ratio (SNR) less than 2. The linear curve fit in Figure 3 represents Eq. 1 for the limit where the fluorescence measurement volume is proportional to the *pixel area x drop diameter,* and can be used to find the expected signal at a smaller drop diameter. For *f#* 2.8, particles less than 104 μm diameter will give a fluorescence signal below the desired SNR of two. Similarly for f# 4, 213 μm defines the lower limit for detectability. In both cases, the limiting fluorescence diameter is greater than the pixel dimension as required. Equ. (1) can be used to estimate the lower identifiable limits in the spray experiments where the beam sheet intensity was 2.2 times less and the

magnification was 0.1. The lower limit under those conditions for an *f#* of 2.8 is 189 μm and 387 μm for an *f#* of 4.

The *f#* experiment was repeated for scattering of the 532*nm* beam. The experimental parameters were the same as above except both fluorescence and scattering from the drop contributed to the signal. The drop size estimated from the images was *3.3 mm ± 13%*, slightly larger than the expected *2.8mm* diameter. Scattering was observed from the portion of the drop on which the laser beam was incident. The size of this region changed with *f#*, but the maximum scattering intensity was insensitive to the increase in *f#*, due to saturation of the film. The scattering from the drops at 532*nm* excitation is very useful in identifying the location of drops, by not so in identifying the size.

To determine if the 355*nm* excitation and 532*nm* excitation would result in the same drop size, a series of images were taken with long pass filters used to cutoff the short wavelengths. With no filter primarily scattering from 532*nm* is observed. The 550*nm* filter adequately blocks the scattering and shows a round drop (eccentricity = 1.04), *3.0mm ±10%* in diameter for 532*nm* excitation and a slightly smaller drop (eccentricity = 1.05), *2.7mm ±10%* in diameter for 355*nm* excitation. The maximum fluorescent signal for 532*nm* excitation is about 16% larger than the corresponding 355*nm* excitation.

Effect of Beam Sheet/Drop Size Variation

The laser beam incident intensity, the illuminated drop volume, and the incidence angle of the ray on the drop are important for determining the intensity of the signal collected from the drop. The incident intensity is a function of the location of the drop in the light sheet, both vertically and in the depth of the sheet. The beam sheet thickness for the 355*nm* excitation and various powers of the 532*nm* excitation are shown in Figure 4, normalized by the full width at half maximum (FWHM) of 4.4 mm for the 532*nm* beam at 220*mJ/pulse*. For high laser power, the visible excitation beam sheet is thicker than the 355*nm* sheet. Thus, visible scattering is seen more often than fluorescence.

The results for the higher laser power (220*mJ/pulse* for 532*nm* beam sheet and 130*mJ/pulse* for the 355*nm* beam sheet) are shown in Figure 5. Here the pulse separation between the two beams is 4*ms*. A 2.8*mm* drop is traversed in 1*mm* increments from behind through the light sheets. These drops were ejected from a 22 gauge hypodermic needle at a rate of 6 drops/s and images were taken apart with a resolution of 71 *μm/pixel* at a downstream location of about 160*mm*. The highest velocity of the drops, accelerated by gravity, is around 1.8*m/s*. Fluorescence at 588*nm* from 355*nm* excitation is observed in the upper drop in each frame, while scattering and fluorescence from 532*nm* beam is observed in the lower drop. Filters were not used to taking these images. The scattering of the 532*nm* laser beam by the forward edge of the drop is the first and last signals observed in the sequence. The largest source of this light is reflected light although signals from the rear and top of the drop indicate the effect of internal reflection. Fluorescence from 532*nm* appears before the fluorescence from 355*nm* due to both a wider beam and the increased response of the dye to 532*nm* excitation. The 532*nm* drop measurement indicated elongated drops with an average eccentricity of 1.14, while the 355*nm* measurements were more round with an eccentricity of 1.07.

An important consideration in defining the beam sheet thickness is the size of the particle that is to be measured. If the sheet is very thin relative to the particle, the probability of measuring the true diameter is small. The measured mean drop diameter is related to the beam sheet thickness by the following formula:

$$D_m = ((2/3)^{1/2} D_a^2 + D_a b)/(D_a + b) \quad (3)$$

Where D_m is the measured mean drop diameter, D_a is the actual drop diameter and b is the beam sheet thickness. If the beam sheet is infinitesimal, the measured diameter is 81.6% of the actual diameter. This means that if all the drops where uniformly the same diameter, the images would show a variety of sizes with a mean diameter that is 81.6% of the actual diameter. If the beam sheet is equal to the drop diameter, the measured particle will be 90.8% of the actual particle, while if 10 times the diameter of the drop, the measured drop will be 98.3% of the true diameter. When a variety of drop sizes are to be measured instantaneously, it is important that the measured diameter be as nearly equal

to the true diameter as possible. This would indicate that a wider beam sheet is better than a thin one. In the spray experiments, the 532*nm* beam sheet thickness was maintained at the FWHM of 4.4 mm.

Another reason for a thicker beam sheet is related to the size of the sampling region. Given a number of drops randomly distributed in a volume such that the mean distance between drop denoted is '*s*', then there is a lower limit to the smallest volume that can be sampled and still return the correct number density, which is s^3. Sampling with a beam sheet dimension less than the mean distance between drops may result in underestimating the total number of drops and over-sampling the large drops. In the sprinkler experiment, the laser beam was expanded in only one direction, leaving the sheet thickness equal to the initial beam diameter of 5 mm. The water flow rate was calculated from the measured drop diameters and the mean axial velocity of the drops. The calculated water flow rate matched the rotameter flow rate to within the measurement error.

MEASUREMENTS IN SPRINKLER SPRAYS

Images of fluorescence and Mie scattering from sprinkler sprays are shown in Figures 6 and 7. The images are 84*mm* by 118*mm* sections of the overall imaged area of 25*cm* by 35*cm*. The camera *f#* was 2.8 and the magnification was 0.1. The 355*nm* excitation consistently gives a much redder drop than the 532*nm* excitation, due to the scattered light. The 355*nm* beam precedes the visible by 1*ms*, which was verified using an oscilloscope triggered by a photodiode. The 532*nm* laser power in Figure 6 is 10*mJ/pulse* while the power in Figure 7 is 200*mJ/pulse*. The 355*nm* power of 120*mJ/pulse* and the dye concentration are held constant.

At low 532*nm* laser power, there are clear particle pairs throughout the image. The drops illuminated by the green laser are only slightly more yellow than the red drops, making distinction in colors difficult. Only due to the direction of gravity can the drop sequence be known and the velocity determined. The velocity of the large drops can be easily measured, but almost no small drops are visible. Increasing the 532*nm* laser power to 200*mJ/pulse* improves the color differentiation between the two drops. More particle pairs are indicated but unpaired green drops appear as a result of the higher intensity of scattering. The drop size at low 532*nm* power was the same for both laser beams, while at higher laser powers all 355*nm* drops are smaller than the corresponding 532*nm* drops. Drops illuminated by 532*nm* tend to have three types of images. In the first type, drops are solid or faint green with no fluorescence, indicating that they are at the edges of the beam or caused by secondary scattering of the laser sheet. The second type has a halo of green scattering completely or partially surrounding a fluorescent core. These are most likely small drops inside the light sheet. Finally, large drops have bright green scattering on the incident side of the laser beam while the rest of the drop image is dominated by a yellowish fluorescence that delineates the drop perimeter.

Figure 8 is an enlargement of Figure 7. In this image, two drops appear to coalesce as they fall. The initial UV beam indicates two fluorescence centers that are disconnected while the second visible laser indicates two bright centers with a single surrounding drop that is oblong. The upper most UV illuminated drop measures 1.47 mm or 21 pixels across. The velocity of the drops is easily measured from drop center to drop center. The radial component is 3.3 m/s outward and the axial component is 5.74 m/s downward, resulting in a speed of 6.6 m/s.

Size and Velocity Distributions

Using the technique described above, images of sprinkler sprays from a 8*mm* nozzle at three combinations of flow rates and strike plate cone angles were analyzed. Fluorescence data was obtained using a Quantaray red filter to remove scattering. Thus, directional ambiguity was resolved only by the direction of gravity. A *f#* of 1.2 was used and the magnification was 0.1. As discussed earlier, the minimum fluorescence signal depends on the *f#* of the lens and the magnification. Based on Equ. (1) and Fig. 3, the minimum detectable fluorescence results from a drop of approximately 35μm. The image resolution was dominated by the film resolution resulting in an expected minimum measurable diameter of 158 μm. Based on Kadambi's [4] criterion of 3 pixels per particle, the actual minimum measurable diameter is 210 μm. Although drops of smaller diameters can be detected, their diameters can not be accurately determined.

Particle trajectories are indicated by the instantaneous drop locations in Figure 9 for the three cone angles. The sprays originated at the 0,0 point and were directed downward and outward at an angle determined by the cone angle of the

nozzle. Measurements are made with 5 gpm and a cone angle of 90°, 4 gpm and 120° and 3 gpm and 140°. The corresponding velocities of particle pairs are shown in Figure 10. Very few images are required to determine the flow trajectories, velocities, and statistics of the spray distribution. For example, in this case two images were used.

Figures 11, 12, and 13 describe the spray statistics. In each of these images, the drop sizes below 150μm have been binned together at 100 μm. The lowest resolvable drop size is 200 μm, which is the second bin in the graphs. Figure 11 is the drop size distribution function. The peaks have been normalized to indicate the spread. The 5 gpm and 4 gpm drop distributions are similar, while 3 gpm indicates larger diameter drops that account for a higher percentage of flow. It should be noted again that although the drops cannot be accurately sized, they are observable and therefore the large size bin into which there are placed indicates the possible error in size estimation.

Figure 12 is the cumulative number distribution, where 0.5 represents half of the total particles in the flow. The statistics indicate that over half of the observed particles in the flow are below the accurately measurable limit of the imaging systems. However, the cumulative volume fraction in Figure 13 indicates that these particles carry about 0.2% of the water flow rate. The cumulative number distribution also indicates that the lower flow rates have a higher fraction of larger drops, which is indicated in the cumulative volume fraction graph for 3 gpm.

CONCLUSIONS

In measuring large fields of view, delectability of drop diameters down to $35\mu m$ is possible but size measurement is limited by fluorescence intensity and collection optics parameters. Fluorescence curves indicate that the proper concentrations of dye for maximum fluorescence imaging are around 0.0033 g/l for rhodamine. In order to detect small drops, a low *f#* is desired, however there is limit to the *f#* beyond which the ability to accurately measure size is impeded. Accurate measurements of drop sizes greater than $210\mu m$ were obtained in this work in a field of view of 25cm×35cm by using fluorescence. This measurements is limited only by the film resolution and the standard digital resolution requirement of three pixels per particle. Scattering images did not prove to adequately represent the particle size. The effect of variation of intensity across the beam sheet, depth of focus, and volumetric response of the fluorescence signal combine to give varying drop sizes. These sizes varied by 8% and were observed to give an estimated drop size 7% lower than physical measurements.

Using the technique developed, particle tracking velocimetry and size measurements of water droplets in large-scale sprinkler flows were conducted. Spray patterns, drop velocities and drop sizes were measured to provide data on instantaneous and time averaged water delivery density for three separate spray conditions. Drop sizes were detected down to $35\mu m$ and were accurately measurable down to $210\mu m$. Spray number distributions indicate that many of the drops are below the measurable size, but volume measurements indicate that 99.8% of the flow is carried by drops of measureable size.

REFERENCES

1. McGrattan, K.B. Hamins, A. and Forney, G.P., 1999, "Modeling of Sprinkler, Vent and Draft Curtain Interaction," Sixth (International) Symposium on Fire Safety Science, France.
2. W.D. Bachalo. Experimental Methods in Multiphase Flows. Int. J. Multiphase Flow. Vol. 20, Suppl. pp261-295. 1994.
3. C.R. Tuck, M.C. Butler Ellis, and P.C.H. Miller. Techniques for the measurement of droplet size and velocity distributions in agriculture sprays. Crop Protection. Vol. 16 No. 7. pp619-628. 1997.
4. J.R. Kadambi, W.T. Martin, S. Amirthaganesh, and M.P. Wernet. Particle sizing using Particle Imaging Velocimetry for two-phase flows. Powder Technology Vol. 100. pp251- 259. 1998.
5. D.C. Herpfer, S. Jeng. Planar Measurements of Droplet Velocities and Sizes Within a Simplex Atomizer. AIAA Journal, Vol. 35 No. 1. January. pp127-132. 1997.
6. Z. Cao, K. Nishino, and K. Torii. Measurement of Size and Velocity of Water Spray Particle Uising Laser-Induced Fluorescence Method. Proceedings of the 2nd Pacific Symposium on Flow Visualization. Honolulu, Hi. May 16-19, 1999.

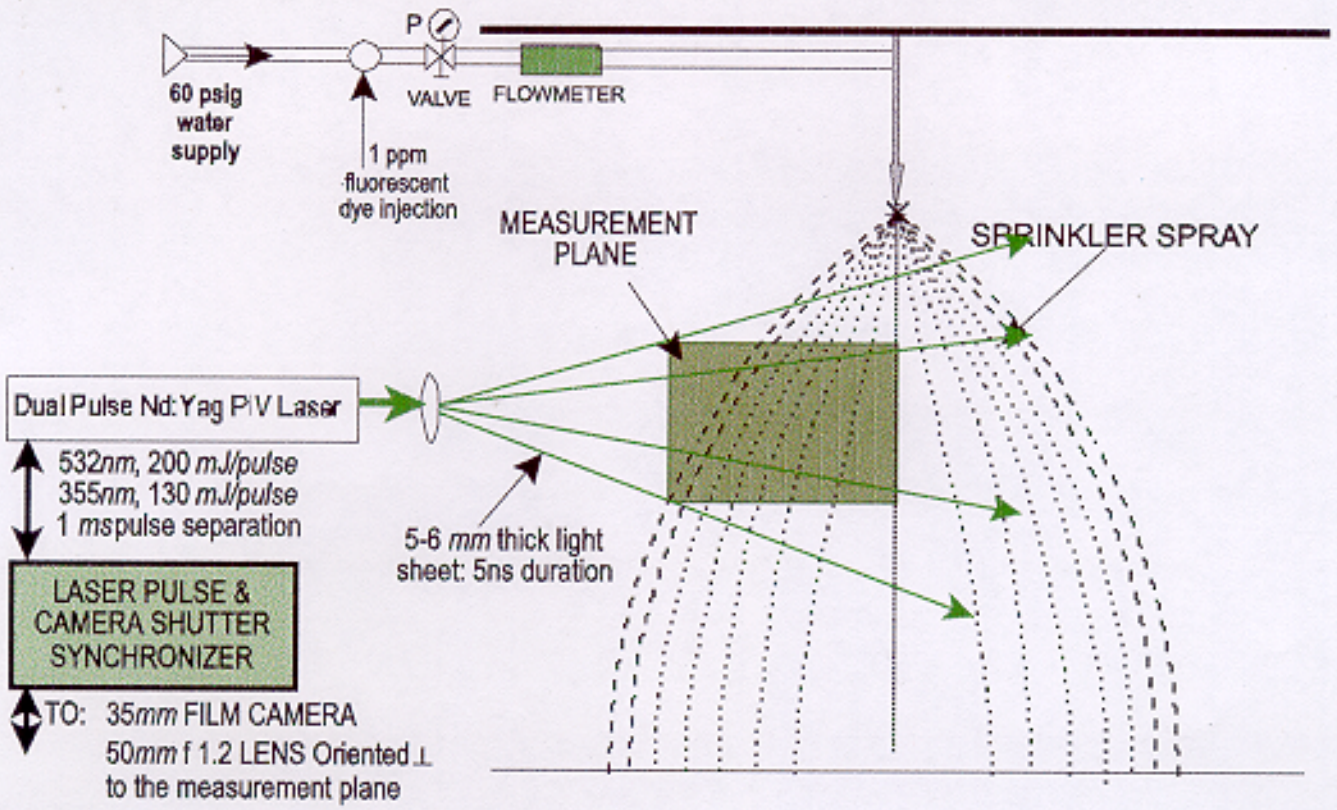

Figure 1. Experimental arrangement for spray measurements.

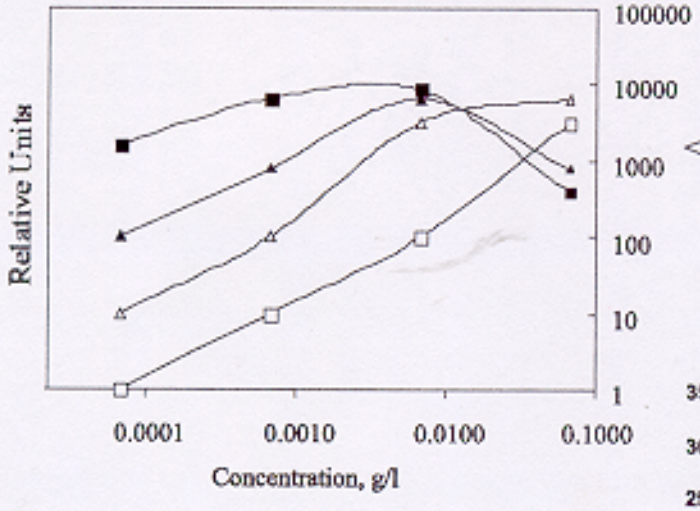

Fig. 2: Relative Fluorescence Emissions from the Tracer dyes for 532nm & 355nm Excitation.
Square - 532 nm excitation, 5 mJ/shot
Triangle - 355 nm excitation, 5 mJ/shot
Rhodamine - closed symbol
Fluorescein - open symbol

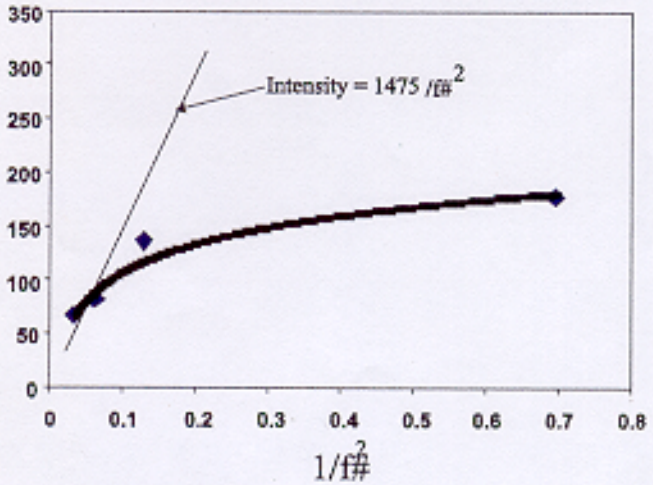

Fig. 3: Fluorescence response from a 2.8 *mm* drop at 355 *nm* excitation. Straight line indicates that intensity is expected to vary inversely with $f\#^2$. However for low $f\#$s the intensity falls considerably below the expected levels due to depth of field effects.

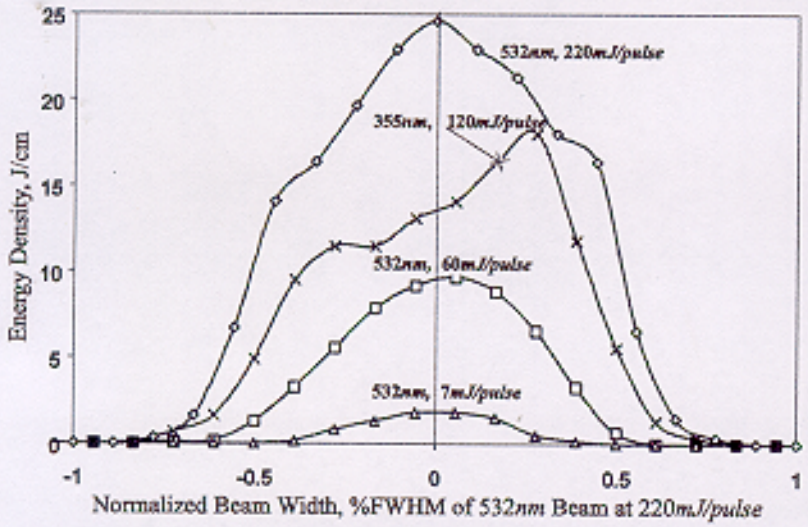

Fig. 4: Relative beam sheet thickness for 355*nm* laser beam at high laser fluence and for 3 different laser fluences of the 532*nm* beam.

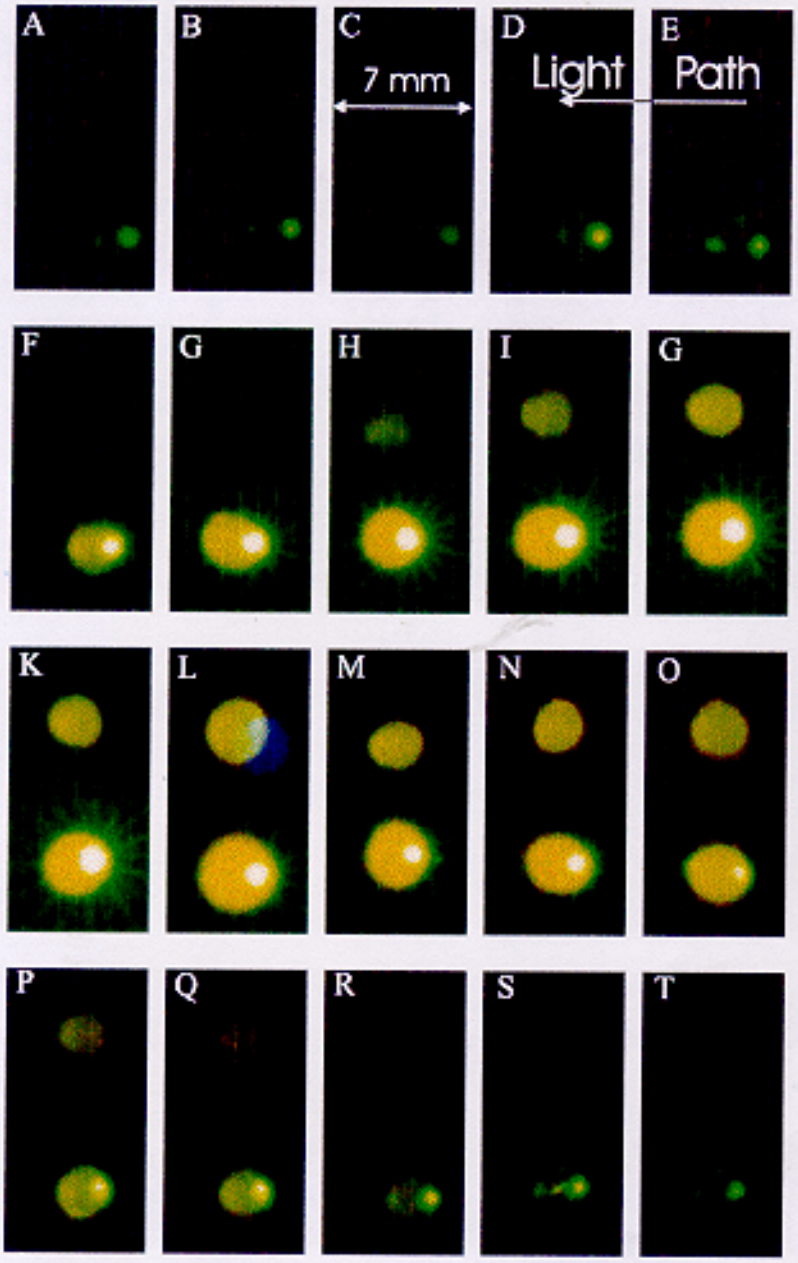

Fig. 5: The 2.8*mm* drop is moved forward from behind the laser sheet in 1*mm* increments. The 532*nm* laser sheet has a FWHM of 4.4*mm* and the 355*nm* laser sheet has a FWHM of 3.6*mm*. Laser power for the 532*nm* beam is 220*mJ/pulse* and for the 355*nm* beam is 130*mJ/pulse*. Fluorescence at 588*nm* from 355*nm* excitation is observed from the upper drop in each frame, while scattering and fluorescence from 532*nm* beam is observed from the lower drop. Filters were not used to taking these images. When the drop is centered in the beam sheets, the drop size as measured by fluorescence from 355*nm* excitation is 2.7*mm*, while the drop size as measured from 532*nm* excitation and scattering is 3.3*nm*. When centered in the 355*nm* laser sheet, some scattering from 355*nm* was detected by the film.

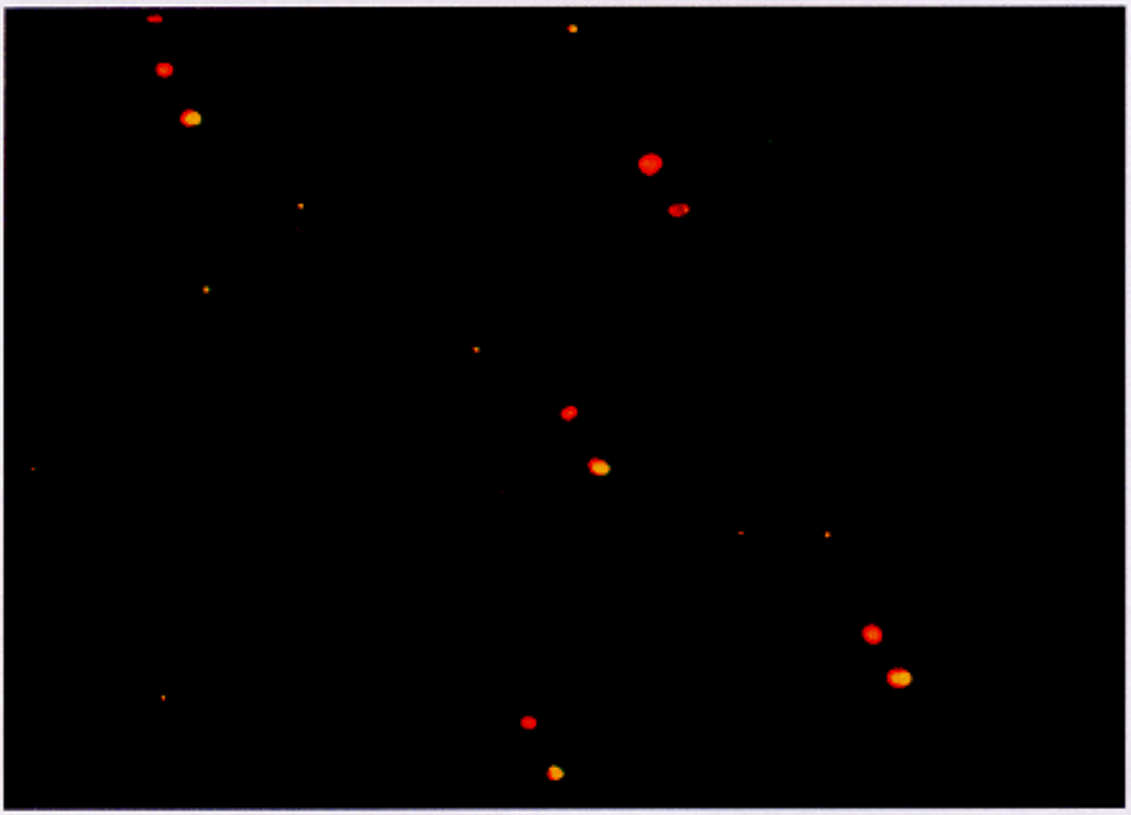

Fig. 6: Low Laser Power at 532nm (10 mJ/shot). High Laser Power at 355nm (120 mJ/shot). Imaged area: 84mmX118mm.

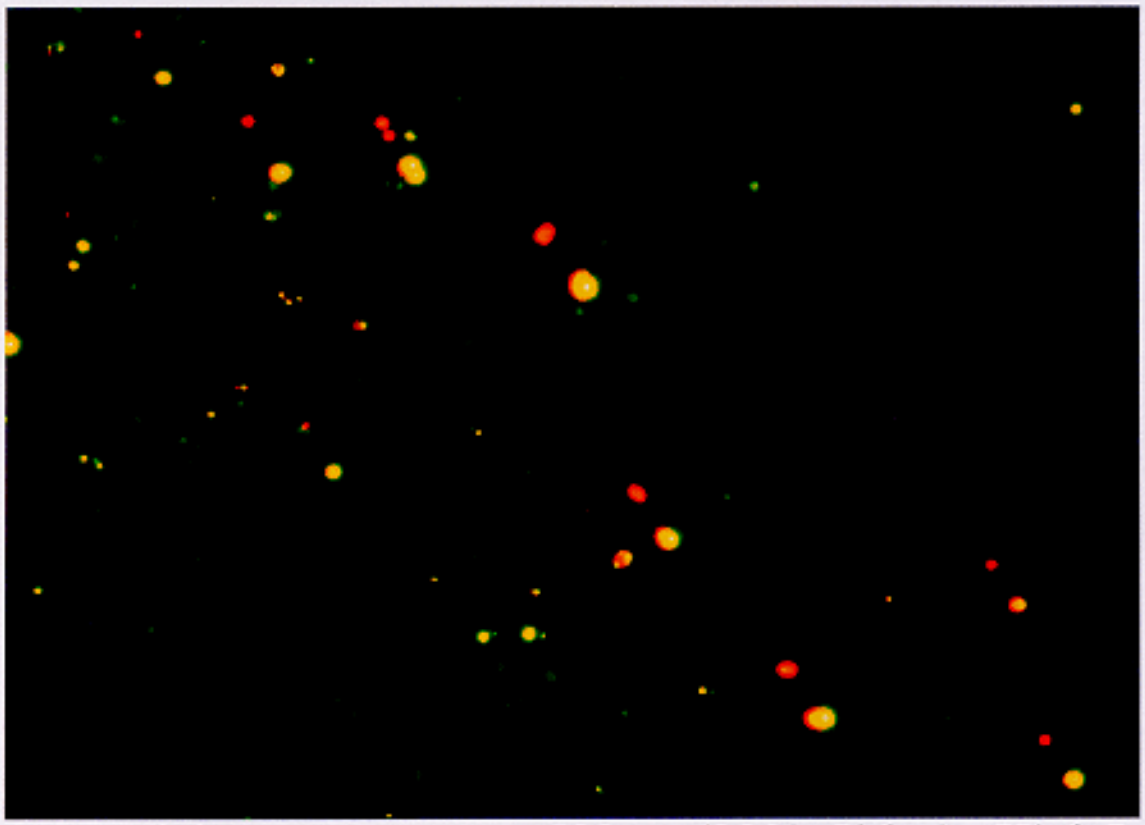

Fig. 7: High Laser Power at 532*nm* (200*mJ/shot*). High Laser Power at 355nm (120*mJ/shot*). Imaged area: 84mmX118mm.

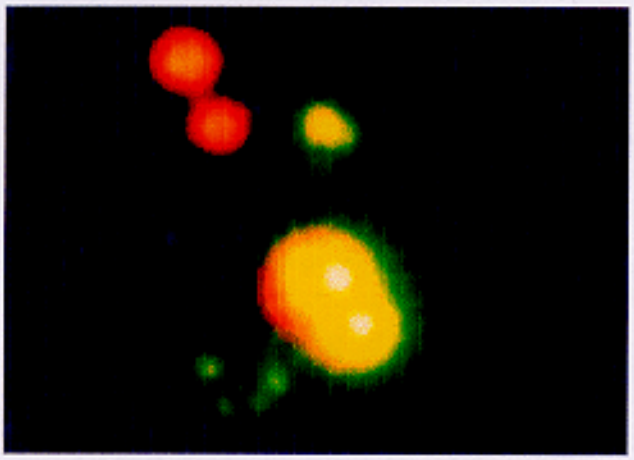

Fig. 8: Enlarged view of a small region of Fig.7. The upper red drop is caused by UV excitation. Its diameter is 1.47mm or 21pixels. The bright yellow drops are caused by visible radiation. A green corona appears due to scattering at the front edge of the drop.

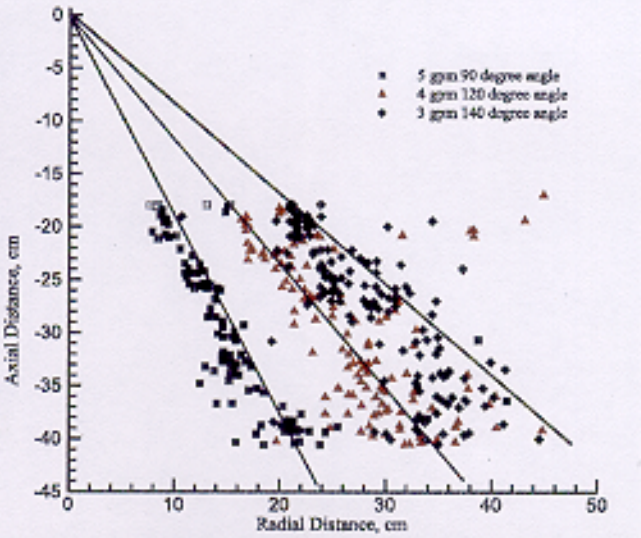

Fig. 9: Drop trajectories for a nozzle with an orifice diameter of 8mm. These trajectories are indicated by 3 lines corresponding to different cone angles of the strike plate that control the spray pattern.

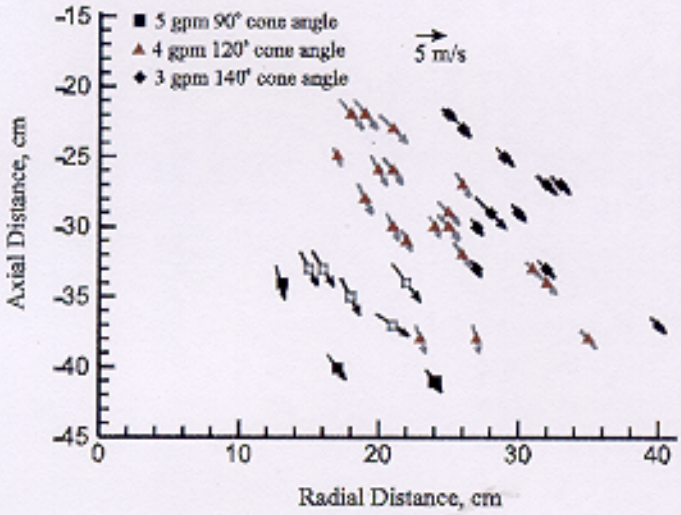

Fig. 10: Drop velocities for a nozzle with an orifice diameter of 8mm.

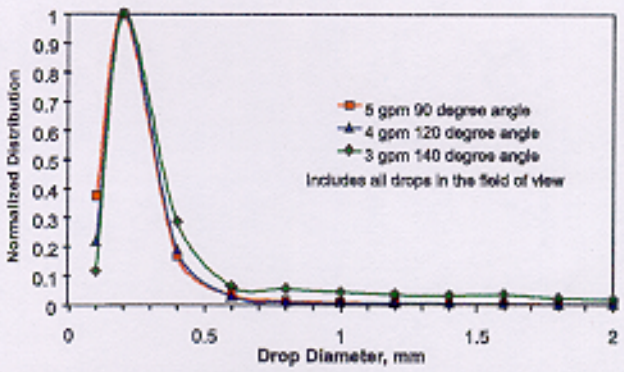

Fig. 11: Drop size distribution for a nozzle of 8 mm dia orifice. Normalized by the maximum number density.

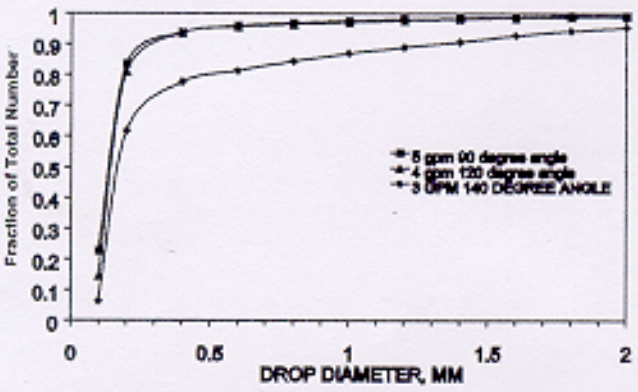

Fig. 12: Cumulative number density distribution for the 8 mm dia. nozzle. Thus, comparatively fewer number of drops are larger than 0.5 mm.

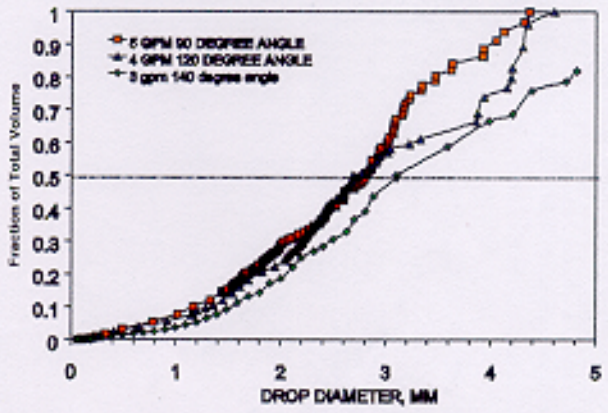

Fig. 13: Cumulative volume fraction distribution for the 8 mm dia. nozzle. The drop diameter at 0.5 is about 2.8 mm, indicating that half the volume of water is carried by larger drops.